

Numerical study of the performance of WIG marine vehicles

Mohamed A. Kotb and Yasser M. Ahmed

Marine Eng. and Naval Architecture Dept., Faculty of Eng., Alexandria University, Alexandria, Egypt

Wing in Ground Effect crafts (WIG crafts) represent a new era in the waterborne transportation. The WIG crafts work near water or ground surfaces and the benefit of operation in ground proximity is manifested in higher lift and lower drag. In this study performance analysis of a simple planar wing with no end plates of a WIG vehicle cruising over and in proximity to ground surface is numerically studied. Lift and drag characteristics in two different modes of operation are also studied. These are in and off ground conditions. The numerical study is based on vortex lattice method. An image wing spaced below the actual wing simulated the ground effect. Results are compared to existing analysis and experimental data.

تمثل المركبات البحرية من نوع الـ WIG مرحلة جديدة في النقل البحري. وهذه المركبة البحرية تعمل في الهواء قريبا من سطح الماء حيث تكون قوة الرفع الديناميكية المتولدة بواسطة أجنحة خاصة كبيرة وذلك كلما زاد اقتراب المركبة من سطح الماء. في هذا البحث تم دراسة أداء هذا النوع من المركبات رقميا وذلك من حيث قوة الرفع والإعاقة الديناميكية. الطريقة الرقمية المستخدمة تعتمد على نظرية شبكات الرفع الدورانية مع تمثيل سطح الماء عن طريق صورة للمركبة في الجانب الآخر للماء. تم مقارنة النتائج بمثلاتها من الدراسات العملية والتحليلية.

Keywords: WIG craft, Ground effect, Dynamic lift, Effective aspect ratio, Induced drag

1. Introduction

Marine vehicles are classified according to different criteria such as navigational route, working area with respect to the water surface, material of construction, mission, lifting force... etc.

The most recent member, which has joined marine vehicles family, is wing in ground effect vehicle, or WIG (fig. 1), which is the official term adopted by the International Maritime Organization (IMO) and International Civil Aviation Organization (ICAO) for a marine craft using ground effect as a mean of lift.

A wing in ground effect vehicle (WIG) is a craft that is especially designed to take advantage of the reduced drag and increased lift of ground effect. Therefore a WIG vehicle will always fly close to the surface, fig. 2. Although it is called *ground effect*, most WIG vehicles only fly over water, but some are amphibious.

The main difference between a WIG and Air Cushion Vehicles (ACV's) or Surface Effect Ship (SES's) is that a WIG vehicle rides on a dynamic air cushion as opposed to a hovercraft, which rides on a static air cushion. The WIG generates lift by forward speed, but

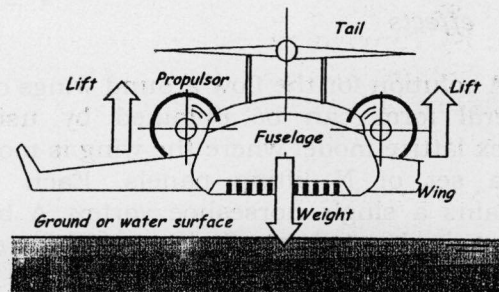


Fig. 1. Wing in ground effect craft WIG.

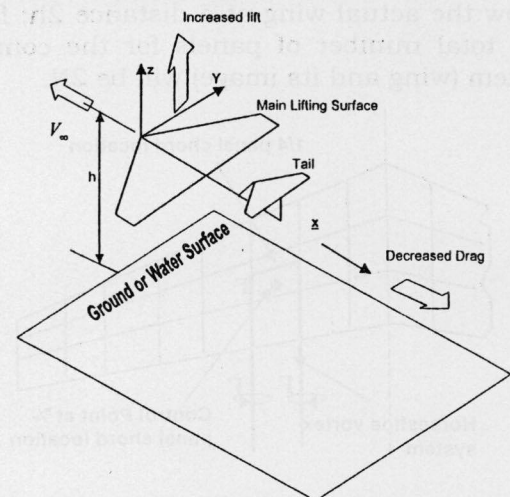


Fig. 2. Wing in ground effect vehicle.

the hovercraft has fans that continuously blow up the cushion. This is why a WIG is much more (fuel) efficient than a hovercraft.

During the last decades a large number of very different WIG vehicles have been designed and built [1]. Most of these designs were built for military purposes. Commercial production already started in the USA [2], and Australia [3].

In 1995, the IMO recognized and issued regulations concerning wing in ground effect vehicles [4].

In [5], the authors studied parametrically the effect of ground proximity on the supporting lift. Simple explanations were given. The effect of main geometrical particulars is studied. Formula for apparent or effective aspect ratio based on lift characteristics was derived.

In this paper, numerical investigation is carried out to predict performance details of a WIG vehicle in different operating conditions.

1.1. Vortex lattice method including ground effects

A solution for the flow around wings of any general form can be obtained by using a vortex lattice model where the wing is modeled as a set of N lifting panels. Each panel contains a single horseshoe vortex. A bound vortex is located at the panel $1/4$ chord position with two trailing vortex lines shed from each end, fig. 3. The ground is simulated by an image of the whole wing located right below the actual wing at a distance $2h$; fig. 4. The total number of panels for the complete system (wing and its image) will be $2N$.

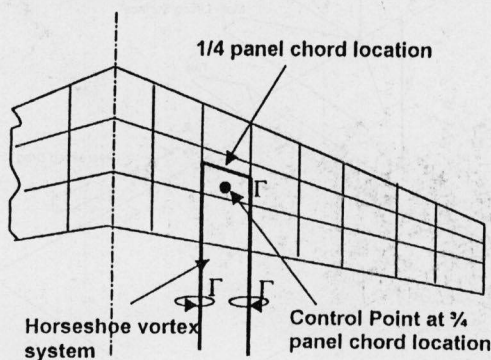


Fig. 3. Wing divided into lifting panels with a horseshoe vortex.

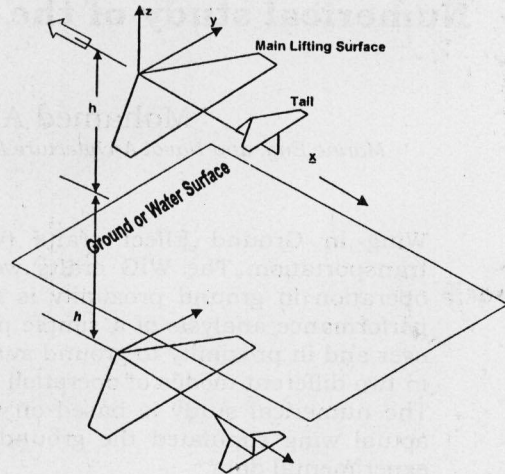


Fig. 4. Ground simulated through an "image wing".

The required strength of the bound vortex on each panel is calculated by satisfying the condition of zero flow normal to the surface. For each panel the condition is applied at the $3/4$ -chord position along the centerline of the panel. The normal velocity is made up of a free stream component and an induced flow component w_i .

$$V_\infty \sin(\alpha) + w_i = 0. \quad (1)$$

This induced velocity component is a function of strengths of all vortex panels on the wing and its image.

$$w_i = \sum_{j=1}^N A_{ij} \Gamma_j. \quad (2)$$

Thus for each panel an equation can be set up which is a linear combination of the effects of the strengths of all panels. A matrix of influence coefficients is created, multiplied by the vortex strengths and equated to the vector of free stream effects.

$$\sum_{j=1}^N A_{ij} \Gamma_j = -V_\infty \sin(\alpha). \quad (3)$$

The influence coefficients A_{ij} will represent the induced flow on panel i due to the vortex on panel j . Biot-Savart law can be used to calculate the induced velocity due to the three component vortex lines [6]. Fig. 5 illustrates

the induced velocity components at panel i due to bound vortex at panel j . The z component is given by:

$$w_i = \frac{\Gamma_j}{4\pi|\bar{r}_1 \times \bar{r}_2|^2} \left(\frac{\bar{r}_0 \cdot \bar{r}_1}{r_1} - \frac{\bar{r}_0 \cdot \bar{r}_2}{r_2} \right) (\bar{r}_1 \times \bar{r}_2)_z \quad (4)$$

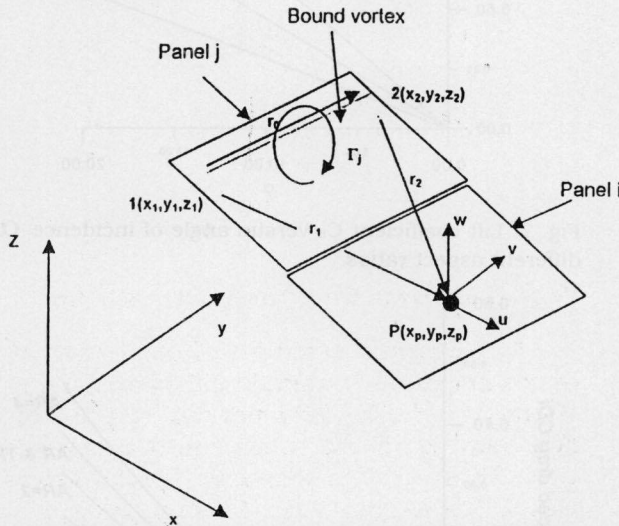


Fig. 5. Velocity components induced by a bound vortex.

A solution for the strength of the vortex lines on each panel is found by solving the matrix of equations in terms of the free-stream V_∞ , the wing incidence angle α , and the wing dimensions.

The lift for the wing at a given angle of attack will be obtained by integrating the panel lift distribution where the lift on a particular panel can be found using the Kutta law; hence:

$$L = \sum_{i=1}^N \rho V_\infty \Gamma_i \Delta y_i \quad (5)$$

The downwash velocity induced on a panel can be calculated once the strength of the wing loading is known. The variation between local flow angles for the panel and the free stream velocity can be found. A consequence of this downwash flow is that the direction of action of each panel's lift vector is rotated relative to the free stream direction. The local lift vectors are rotated backward and hence give rise to a lift induced drag. By integrating the component of panel lift coefficient that

acts parallel to the free stream across the span then the induced drag can be found.

$$D = \sum_{i=1}^N \rho V_\infty \Gamma_i \sin(\alpha_i) \Delta y_i \quad (6)$$

The induced flow angle α_i represents the amount of rotation of the lift vector backward and must be calculated from the velocities induced on the bound vortex of the panel by other panels and the free stream.


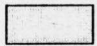
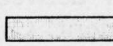

A computer code based on the method above is written and used to calculate the flowfield as well as lift and induced drag on a planar wing moving at a height h above the ground at different attitudes.

The program assumes inviscid, steady and incompressible flows. The model is restricted to flat plate wings. The model can handle geometrical configurations such as sweep, dihedral, tapered and wing tail geometries. The model is used to provide some preliminary results to show the effects of heights above the ground on the lift, drag, and lift to drag ratio for an isolated wing. The model also can be used to provide some preliminary simulations of a wing tail configurations. Details on the code and the vortex lattice method derivations can be found in [7].

2. Case study

Rectangular planforms with Aspect Ratios, (AR), of one, two and four and a tapered planform with a taper ratio (C_r/C_t) of two were examined. Details of configurations studied are shown in table 1.

Table 1
Wing geometrical particulars

Case	Planform	Aspect ratio	Taper ratio
	Square	1	1
	Rectangle	2	1
	Rectangle	4	1
	Tapered	2	2

2.1. Results

2.1. 1. Wings out of ground effects

Wing numerical results regarding lift, drag, and lift/drag ratio in free flight, that is away from the ground effect are first obtained to form a basis for comparison.

Fig. 6 depicts the lift curve slope, $(dC/d\alpha)_{\alpha=0}$, versus aspect ratio. Experimental [8], as well as, other analytical results [9,10] are shown on the same plot. Results show that lift curve slope increases with increasing aspect ratio.

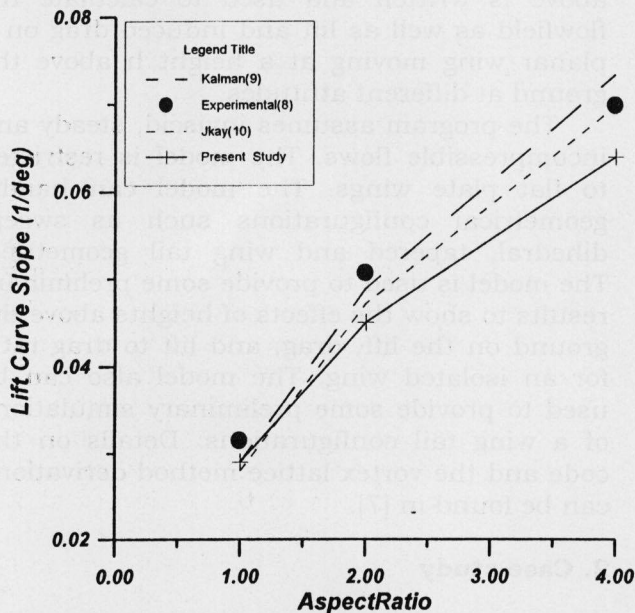


Fig. 6. Lift curve slope versus aspect ratios for rectangular wing.

Fig. 7 represents the lift coefficient as a function of incidence angle at different aspect and taper ratios. It is seen that the lift coefficient increases with both the aspect ratio and the angle of attack and the effect of tapering the wing on the lift value while maintaining the same aspect ratio was found to be almost negligible. Present study results are in good agreement with other calculations and deviate from experimental data in the range of 5 to 9 %.

Curves representing the relation between drag due to lift (induced drag coefficient, C_{Di}), and the angle of attack at different aspect and taper ratios are shown in fig. 8. It is seen that the induced drag coefficient increases with the increase of aspect ratio at the same angle of

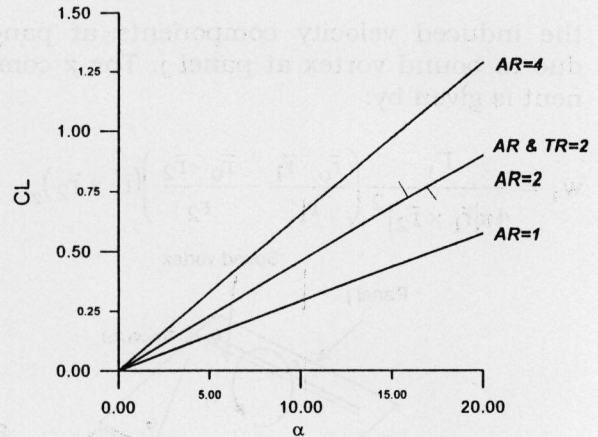


Fig. 7. Lift coefficient C_L versus angle of incidence α for different aspect ratios.

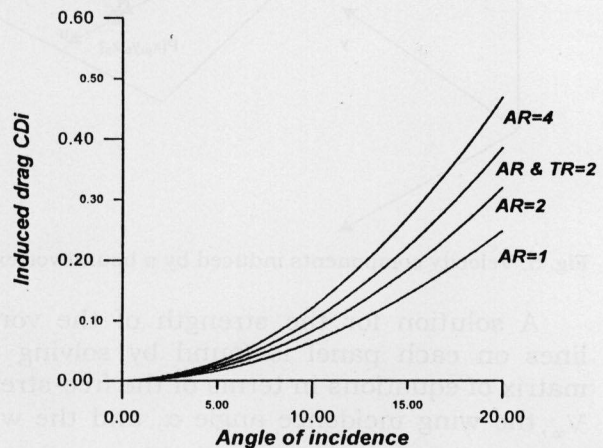


Fig. 8. Drag coefficient versus angle of incidence for different aspect ratios.

attack. This is explained as the increase of the aspect ratio increases the lift coefficient at the same angle of attack and consequently increases the resulted induced drag coefficient. Tapered wing experiences more induced drag than the rectangular wing of the same aspect ratio. Fig. 9, which is a drag polar plot, emphasizes that the increase of the induced drag coefficient with the decrease of the aspect ratio at the same value of the lift coefficient. Induced drag is also plotted versus the square of the lift coefficient in fig. 10 in away to measure how efficient is the plan form (or the effect of departure from elliptic lift distribution on the induced drag). Linear relations were obtained for the induced drag variation with the square of the lift coefficient. The slope, which is inversely proportional to the wing span efficiency effect in off ground effect

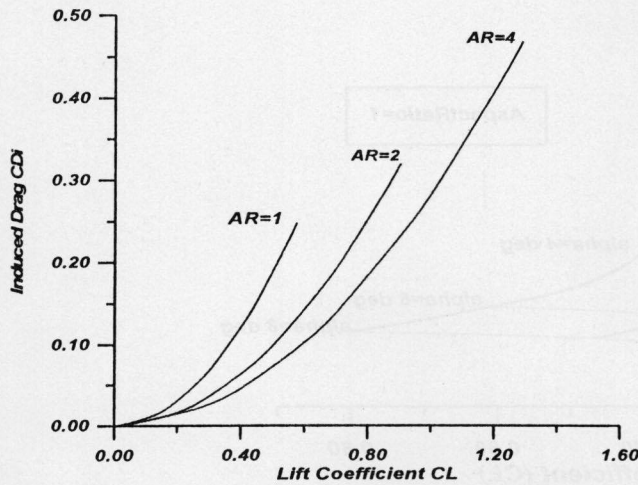


Fig. 9. Induced drag for rectangular wings versus lift coefficient at different aspect ratios.

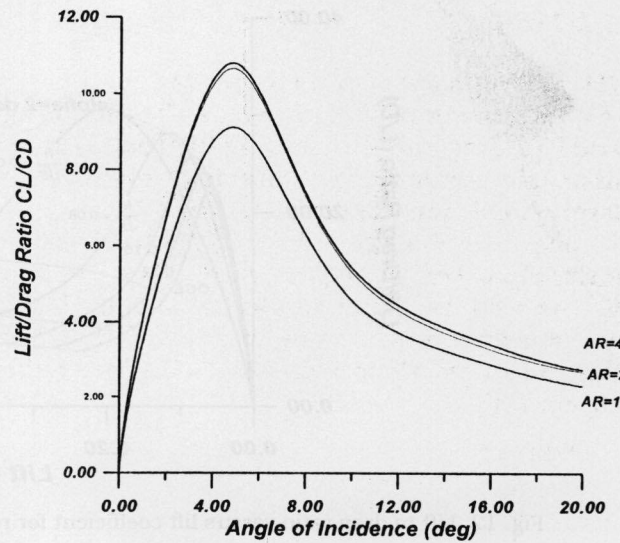


Fig. 11. Lift to drag ratio versus angle of incidence for rectangular wings for different aspect ratios at off ground condition.

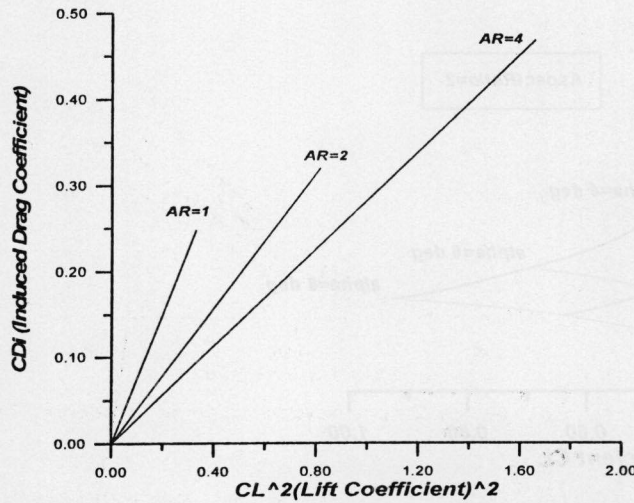


Fig. 10. Induced drag versus lift coefficient squared for different aspect ratios at off ground conditions.

condition, will be used later to assess the effect of ground proximity.

Fig. 11 shows the effect of the angle of incidence and the aspect ratio on the lift to drag ratio, where the ratio increases with the increase of the aspect ratio while it has a maximum of about 10 at an incidence of about 5 degrees.

2.1.2. Wings in ground effect

In figs. 12 through 15, the ratios of lift to drag (L/D) are plotted as functions of C_L over a range of heights above the ground and wing aspect ratios. The height ratio is expressed as

h/\sqrt{S} instead of h/c so to include the effect of aspect ratio. This parameter has been used in [11,12] to present experimental and computational lift drag results for WIG vehicles.

Contours of constant incidence angles are sketched on the same plots. Lift/drag variation at off ground effect is also included in these plots. Results of these figures show that maximum lift drag ratio increases with the increase of both wing loading (in terms of lift coefficient C_L), and wing aspect ratio. It also increases with the decrease of height ratio. It also shows that tapered planform produces nearly the same lift drag ratio as that for the rectangular planform of the same aspect ratio.

The rate of change of maximum lift drag ratio $(C_L/C_D)_{max}$ with respect to both lift coefficient C_L and height ratio h/\sqrt{S} as a function of aspect ratio is shown in fig. 16.

Fig. 17 represents lift drag ratio as a function of height above the ground for different aspect ratios at the same cruising attitude (2° in this case). This figure shows clearly how lift drag ratio increases with the decrease of the height above the ground, and increase of wing aspect ratio.

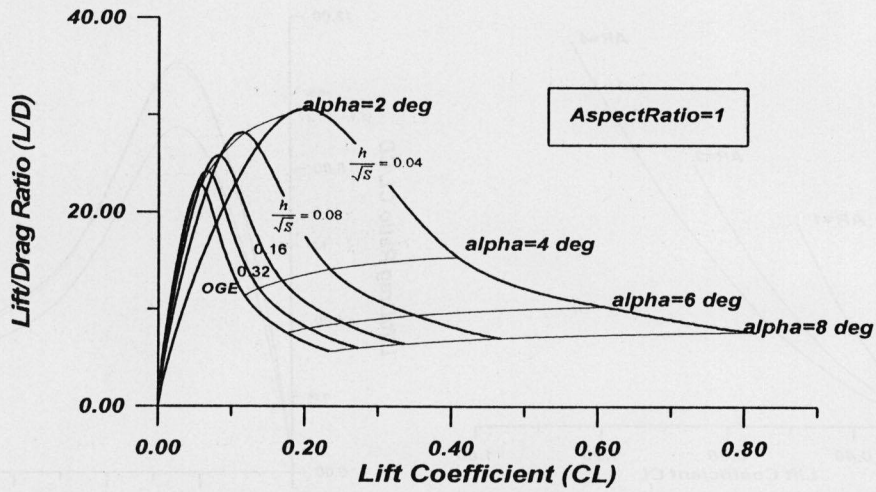


Fig. 12. Lift to drag ratio versus lift coefficient for rectangular wing at different height ratios (aspect ratio=1).

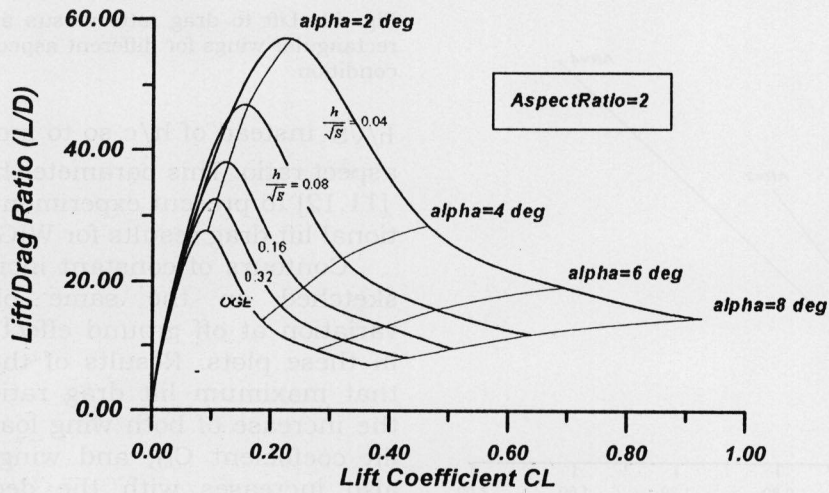


Fig. 13. Lift to drag ratio versus lift coefficient for rectangular wing at different height ratio (aspect ratio=2).

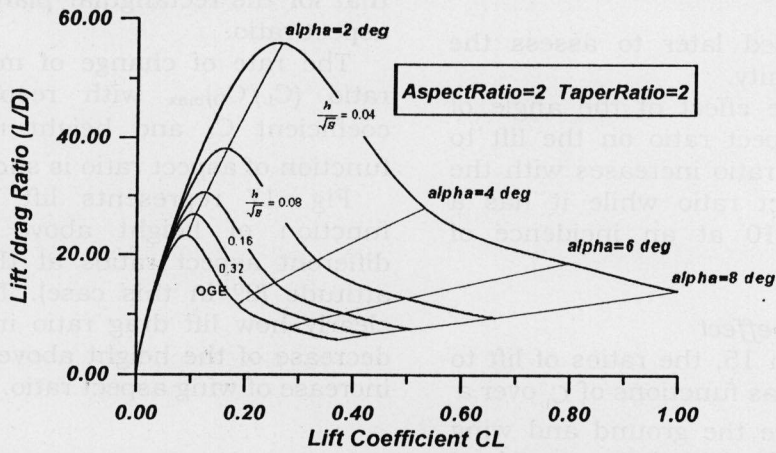


Fig. 14. Lift to drag ratio versus lift coefficient for tapered wing at different height ratios (aspect ratio=2, taper ratio=2).

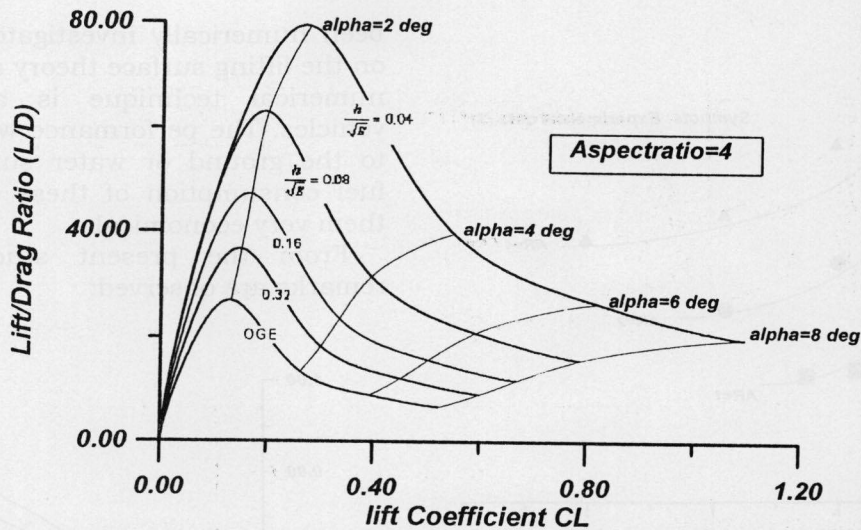


Fig. 15. Lift to drag ratio versus lift coefficient for rectangular wing at different height ratios (aspect ratio=4).

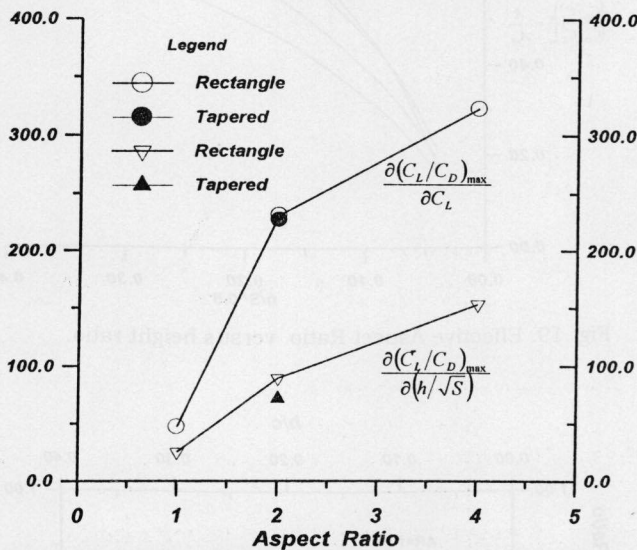


Fig. 16. Maximum lift-drag ratio derivatives with respect to wing loading and height ratio versus aspect ratio.

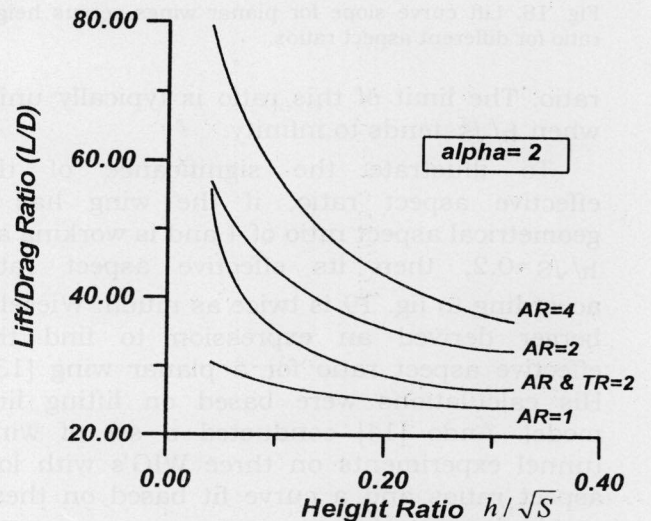


Fig. 17. Lift/drag ratio versus height ratio for planar wings of different aspect ratios.

Fig. 18 shows the variation of lift curve slope with height ratio for three different aspect ratios. Results compared well with experimental data of ref. [8]. The plots show clearly how the ground proximity dramatically increases lift curve slope particularly for heights less than 0.25 wing chord.

The increase of lift drag ratio with decrease of ground height can be interpreted as equivalent to virtually increased aspect ratio. To illustrate this, the parameter $(C_D/C_L^2)_h$ at any cruising height h normalized by its

counterpart $(C_D/C_L^2)_\infty$ at free cruising condition is plotted versus height ratio h/\sqrt{S} in fig. 19. This ratio $(C_D/C_L^2)_h / (C_D/C_L^2)_\infty$, used in this plot is equivalent to the ratio between the wing geometric aspect ratio, and the virtually increased effective aspect ratio AR_g/AR_{eff} where AR_g is the geometrical aspect ratio while AR_{eff} is the corresponding apparent or effective aspect ratio due to ground proximity. The figure is made for three different aspect ratios and one single tapered

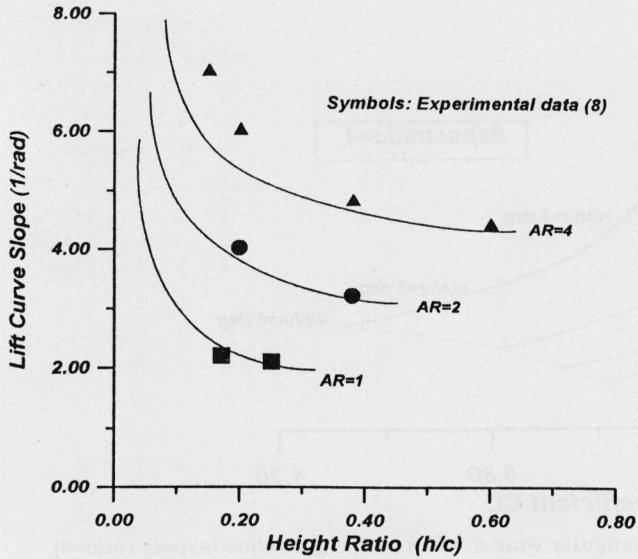


Fig. 18. Lift curve slope for planar wings versus height ratio for different aspect ratios.

ratio. The limit of this ratio is typically unity when h/\sqrt{S} tends to infinity.

To illustrate the significance of the effective aspect ratio, if the wing has a geometrical aspect ratio of 4 and is working at $h/\sqrt{S}=0.2$, then its effective aspect ratio according to fig. 19 is twice as much. Wieselsberger derived an expression to find the effective aspect ratio for a planar wing [13]. His calculations were based on lifting line model. Ando [14] conducted a set of wind tunnel experiments on three WIG's with low aspect ratios and a curve fit based on these results is suggested.

Wieselsberger model when compared to collection of experimental data reported by Hoerner [15] was shown to under predict the effective aspect ratio when working close to ground.

Calculations of fig. 19 are compared to both Wieselsberger model, Ando's experimentally based model, as well as Lockheed test results in figs. 20-22, respectively, for three different aspect ratios.

3. Conclusions and recommendations

In this paper, the performance of WIG craft as potentially promising marine vehicles has

been numerically investigated. Detailed study on the lifting surface theory and its associated numerical technique is applied to these vehicles. The performance when working near to the ground or water surface reduces the fuel consumption of these crafts and makes them very economical.

From the present study the following remarks are observed:

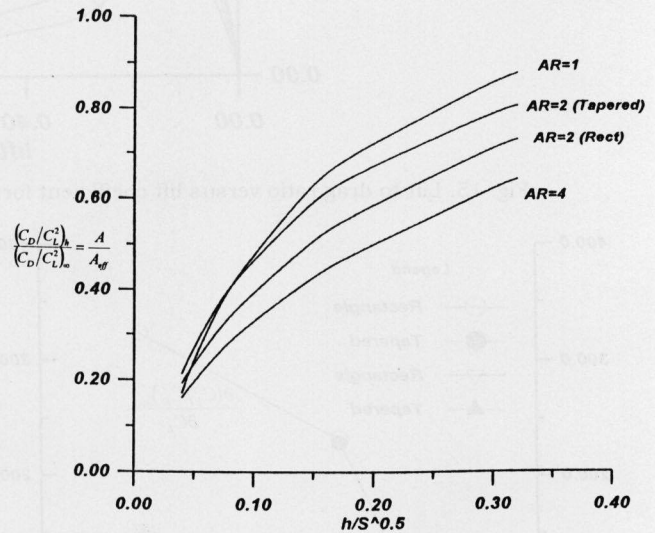


Fig. 19. Effective Aspect Ratio versus height ratio.

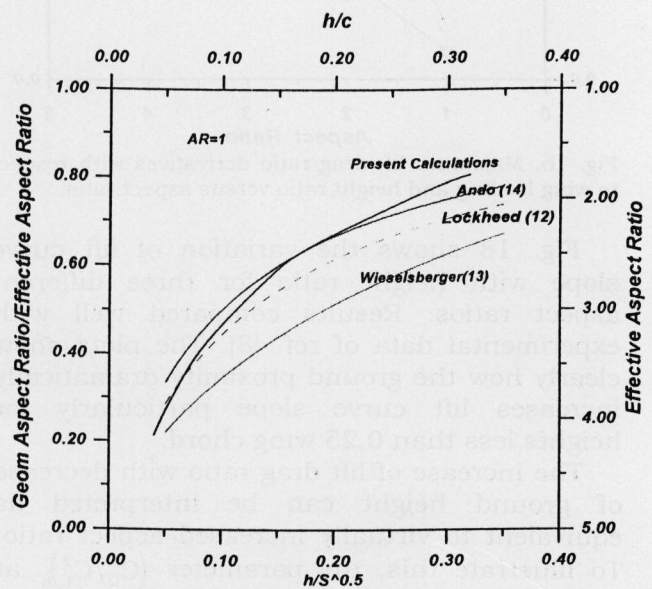


Fig. 20. Effective aspect area ratio versus height ratio at aspect ratio=4.

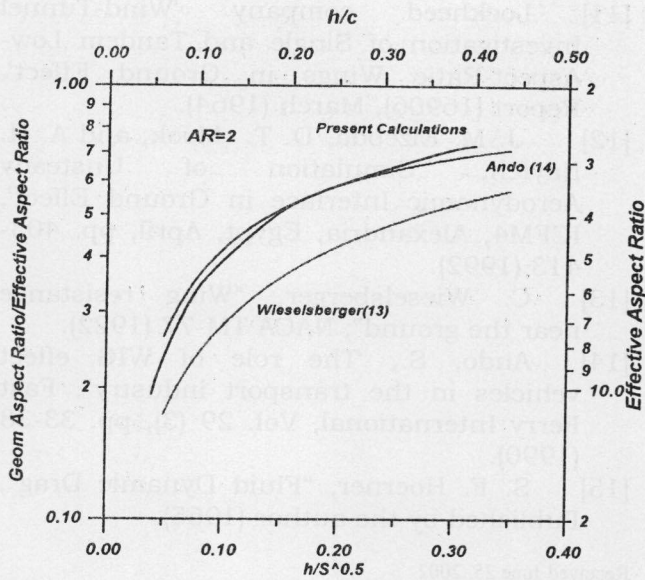


Fig. 21. Effective aspect area ratio versus height ratio at aspect ratio=2.

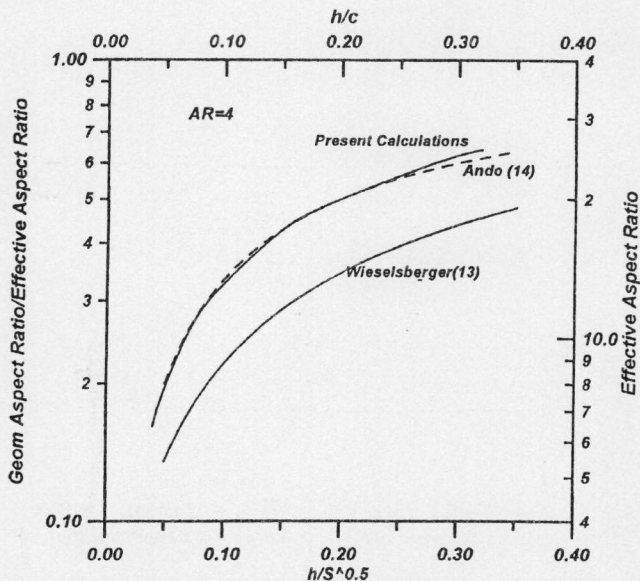


Fig. 22. Effective area ratio versus height ratio at aspect ratio=1.

1. Working near the ground has two pronounced effects. These are increased lift and reduced induced drag, hence increased lift/drag ratio.
2. This favorable effect is interpreted in the form of increased wing span or aspect ratio.
3. Through simple inviscid, and incompressible numerical analysis (VLM combined with image technique) on planar

wings, L/D parameter was calculated and compared to its free flight counterparts.

4. Design performance charts were prepared which could be used to assess vehicle performance such as $(L/D)_{max}$ and its location and cruising altitude. These charts could also be used a preliminary design tool to assess the appropriate cruising altitude for known given vehicle weight and/or vehicle geometrical characteristics in flying altitude.

5. Results yielded a simple graph through which one can assess the effective aspect ratio of the vehicle at any given operating condition.

6. Effective aspect ratio in terms of geometric wing dimensions and cruising altitude are compared with existing published experimental and analytical data. Good agreement was obtained.

7. Finally, it is recommended to include other factors such as camber and thickness, which should improve the performance predictions.

Acknowledgments

The authors would like to extend their sincere thanks to Professors A. S. Sabet and A. Elbadan, for the review of this paper and for their helpful suggestions throughout this work.

References

- [1] M. A. Kotb, "Ultra High Speed Advanced Marine Vehicles - State of the Art", Reviewing Article, Naval Architecture and Marine Engineering Department, internal Report, Alexandria University, July (1999).
- [2] The home Page of the USA Xtreme Xplorer. Available: <http://www.amphistar.com>.
- [3] Flightship; www.flightship.net
- [4] A. I. Bogdanov, "Development of IMO safety requirements for a new high-speed going transportation-WIG craft", Center Marine Research and Design Institute Ltd., Russia (1995).
- [5] M. A. Kotb, and Y. A. Abdel Razek, "Parametric Study of Dynamic Supporting Force of WIG Marine Vehicles," Alexandria Engineering Journal, Vol.41(5) (2002).
- [6] J. B. Bertin, & M.L. Smith, Aerodynamics for Engineers, Prentice Hall, Inc., Englewood Cliffs (1979).

- [7] Y. M. Ahmed, "Study of Ground Effect Marine Vehicles with Particular Reference to Wing in Ground Effect WIG", M.S. Thesis, Naval Architecture and Marine Engineering Department, Alexandria University, Dec. (2000).
- [8] J. Kay, W.H. Mason, W. Durham, F. Lutze, and A. Benoiel, "Control Power Issues in Conceptual Design: Critical Conditions, Estimation Methodology, Spreadsheet Assessment, Trim and Bibliography," VPI-Aero-200, November (1993).
- [9] T. P. Kalman, W. P. Rodden, and J. Giesing, "Application of the Doublet-Lattice Method to Nonplanar Configurations in Subsonic Flow," *Journal of Aircraft*, Vol. 8 (6), pp. 406-415 (1971).
- [10] W. H. Mason, "Applied Computational Aerodynamics, Chapter 6: Aerodynamics of 3D lifting Surfaces through Vortex Lattice Methods", VPI-SU, Blacksburg, VA24061 (1997).
- [11] Lockheed company 'Wind-Tunnel Investigation of Single and Tandem Low-Aspect-Ratio Wings in Ground Effect', Report (16906), March (1964).
- [12] J. M. Elzebda, D. T. Mook, and A. H. Nayfeh, 'Simulation of Unsteady Aerodynamic Interface in Ground Effect', ICFM4, Alexandria, Egypt, April, pp. 403-413 (1992).
- [13] C. Wieselsberger, "Wing resistance near the ground"; NACA TM-77 (1922).
- [14] Ando, S., 'The role of WIG effect vehicles in the transport industry', *Fast Ferry International*, Vol. 29 (3), pp. 33-38 (1990).
- [15] S. F. Hoerner, "Fluid Dynamic Drag", Published by the author (1965).

Received June 25, 2002
Accepted August 3, 2002

